Simulations of nonlinear quantum damping using the positive P representation

A. M. Smith and C. W. Gardiner

Department of Physics, University of Waikato, Hamilton, New Zealand

(Received 28 September 1988)

We present here an extensive study of the technique of numerical simulations, applied to the solution of a system of equations obtained by the positive P representation. The model we introduce to aid in these investigations has the distinct advantage of an immediate physical interpretation. In these simulations we experience the divergent trajectory or "spike," noted by other authors; however, due to the simplicity of our equations, we are able to categorize and explain these spikes. Finally, we report a disturbing anomaly in some of the simulation results which indicates a possible problem with the use of the positive P representation.

I. INTRODUCTION

Many recent studies in quantum optics have resulted in systems of equations which are both coupled and nonlinear, and hence cannot be easily solved by analytic methods. Authors[1] have then attempted to find solutions by direct numerical simulation of the equations in phase space. It is now well known that the use of traditional Glauber-Sudarshan P representation as a description of the system in phase space very frequently leads to a Fokker-Planck equation for the P function possessing nonpositive definite diffusion. However, this problem has been addressed by Drummond and Gardiner,[2] who introduced a generalized P representation which allows a better-behaved phase-space description. One form of this, called the positive P representation, enables the choice of a Fokker-Planck equation with positive semidefinite diffusion to be made in all situations. This is achieved by removing the explicit conjugacy between some variables, and results in a phase-space representation in a doubled dimension.

Equations based on the positive P representation have now been used to study the stationary and dynamic behavior of physical systems. Of central interest is how the increased dimensionality of the phase space affects the time behavior of the system. Early researchers have noted the occurrence in their simulations of numerical "spikes," where an individual trajectory shoots out into the extra nonclassical phase-space dimensions towards infinity. The question that must be addressed is whether these spikes are an actual quantum effect, an intrinsic result of the increased dimensionality, an artifact of the numerical integration scheme, or perhaps some combination of these.

Many of the earliest attempts in stochastic integration were based on an extension of Euler's algorithm, which, because of its poor stability properties, may have led to numeric instabilities. With this in mind, Klauder and Petersen[3] devised Runge-Kutta methods of stochastic integration which lead to improved local-order accuracy. In the recent paper by McNeil and Craig,[4] an unconditionally stable numerical method for nonlinear stochastic equations was developed which removed all the spikes from their system. However, we feel that, although an improved integration scheme may remove one of the sources of the spikes, there are other reasons for their existence much more intimately related to the nature of the expanded phase space. Indeed, in this study of the parametric oscillator by Wolinsky and Carmichael,[5] it was shown that the trajectories of the simulation are naturally confined to a bounded manifold, and spikes only occur when the trajectories stray outside this region. Of course in most physical systems it is not possible to easily specify the required manifold, if indeed there is one. It is therefore necessary to determine more generally the nature of these spikes, and so in this paper we hope to give a greater understanding of how this second class of spikes occurs and what its purpose is in the simulation.

In Sec. II we develop a set of stochastic equations which may then be numerically integrated. Our Hamiltonian model is of a single-mode interferometer which is damped by both linear and nonlinear couplings to a zero-temperature reservoir. The great advantage of this model is that if offers an immediate physical interpretation with which simulation results can be compared, and provides as well a framework in which an explanation of the numerical spikes can be made. Using the positive P representation we transform the master equation in the interaction picture, via its phase-space representation as a Fokker-Planck equation, into a classical process. Using the Ito rules we obtain an equation for the intensity of the cavity mode, which now in addition to the classical dimension contains the extra phase-space dimension required by the quantum noise. This stochastic differential equation is nonlinear, but a change of variables transforms it to a linear equation which has excellent stability properties, and as well, an exact stochastic solution.

Before conducting the simulations it is necessary to make an examination of the various possible stochastic integration schemes (Sec. III). In particular, three methods are discussed: the traditional Euler algorithm, the mixed explicit-implicit method of McNeil and Craig, and a fully implicit difference scheme.

In Sec. IV we use the results of our simulations to make some general statements about stochastic integration using the positive P representation. The spikes referred to above are clearly in evidence, and may be traced to both the type of integration scheme and the more in-

trinsic phase-space spike. We find that large, but finite, excursions into the complex plane are an intrinsic aspect of this model. However, the initial conditions for these excursions can only be provided by the effect of the random noise driving the system from regions in phase space in which the variables are approximately conjugate. Since this involves the surmounting of a barrier this is normally a rather rare occurrence.

However, a potentially far more serious problem with the positive P simulation occurs when we consider the actual time development of the system. If the ratio of the nonlinear to linear damping is too large, we find that the stationary state reached has some nonzero excitation, whereas physically the stationary state should be the vacuum. When there is no linear damping, the stationary state consists of an equal mixture of one- and zero-photon states, unlike the expected result, where the ratio should be the initial ratio of odd to even number states. By directly integrating the stochastic solution of the linear equation we get identical time development, which suggests that we are simulating the equations properly. The master equation itself may be simulated and confirms our physical expectations, as well as indicating that the source of the anomaly probably lies in the positive P representation. Section V presents a short summary and analysis of the simulation results, and in the Conclusion we outline our conjecture as to where the positive P simulations have gone wrong.

Finally in the Appendix, we explore another generalized P representation, the complex P representation, to see if a stationary solution can be found and whether this solution displays the same anomaly as the positive P simulations. It turns out, however, if the potential conditions are treated sufficiently generally, and a requirement on the number-state probabilities is imposed, that the complex P steady-state solution agrees with the physically reasonable solution.

II. STOCHASTIC MODEL

The model we initially wish to consider is a single-mode interferometer of frequency ω described by the operators a and $a^\dagger$, being damped by both linear and nonlinear couplings to zero-temperature reservoirs. The Hamiltonian which describes this process is given by

$$H = \sum_{j=0}^{2} H_j \ ,$$

$$H_0 = \hbar\omega a^\dagger a + \sum_i \hbar\omega_i \Gamma_{nl,i}^\dagger \Gamma_{nl,i} + \sum_j \hbar\omega_j \Gamma_{l,j}^\dagger \Gamma_{l,j} \ ,$$

$$H_1 = \sum_i (a^{\dagger 2} g_{nl,i} \Gamma_{nl,i} + a^2 g_{nl,i}^* \Gamma_{nl,i}^\dagger) \ , \qquad (2.1)$$

$$H_2 = \sum_j (a^\dagger g_{l,j} \Gamma_{l,j} + a g_{l,j}^* \Gamma_{l,j}^\dagger) \ ,$$

where Γ_{nl} and Γ_l are, respectively, the nonlinear and linear reservoir modes. Following the standard analysis,[6] we obtain in the interaction picture a master equation for the density operator ρ in a reference frame rotating at angular frequency ω as

$$\frac{\partial \rho}{\partial t} = \frac{1}{2}\kappa(2a^2\rho a^{\dagger 2} - a^{\dagger 2}a^2\rho - \rho a^{\dagger 2}a^2)$$
$$+ \frac{1}{2}\gamma\kappa(2a\rho a^\dagger - a^\dagger a\rho - \rho a^\dagger a) \ , \qquad (2.2)$$

where κ is the nonlinear decay rate, and $\gamma\kappa$ describes the linear damping rate. The parameter γ is thus defined as the ratio between the linear and nonlinear damping rates, and proves to be important in the results from the simulations.

We now obtain a phase-space description for the system using the positive P representation of Drummond and Gardiner[2] for the density operator

$$\rho = \int d^2\alpha \int d^2\alpha^+ P(\alpha,\alpha^+) \frac{|\alpha\rangle\langle(\alpha^+)^*|}{\langle(\alpha^+)^*|\alpha\rangle} \ , \qquad (2.3)$$

where the α and α^+ variables are to be treated as independent complex variables. This means that we now use a description in an extended four-dimensional phase space. The Fokker-Planck equation thereby obtained explicitly has a positive definite diffusion matrix and can be shown to be

$$\frac{\partial}{\partial t} P(\alpha,\alpha^+) = \left[\frac{\partial}{\partial \alpha}(\frac{1}{2}\gamma\kappa\alpha + \kappa\alpha^+\alpha^2) \right.$$
$$+ \frac{\partial}{\partial \alpha^+}(\frac{1}{2}\gamma\kappa\alpha^+ + \kappa\alpha\alpha^{+2})$$
$$\left. - \frac{1}{2}\left[\frac{\partial^2}{\partial \alpha^2}\kappa\alpha^2 + \frac{\partial^2}{\partial \alpha^{+2}}\kappa\alpha^{+2} \right] \right] P(\alpha,\alpha^+) \ .$$
$$(2.4)$$

The corresponding stochastic differential equations (SDE's) are

$$d\alpha = -\kappa(\frac{1}{2}\gamma\alpha + \alpha^+\alpha^2)dt + i(\kappa)^{1/2}\alpha \, dW_1(t) \ ,$$
$$d\alpha^+ = -\kappa(\frac{1}{2}\gamma\alpha^+ + \alpha\alpha^{+2})dt + i(\kappa)^{1/2}\alpha^+ dW_2(t) \ . \qquad (2.5)$$

It is then possible to obtain a single SDE for the variable representing the intensity of the cavity mode $N = \alpha\alpha^+$. Using the Ito rules

$$dN = d\alpha\,\alpha^+ + \alpha\,d\alpha^+ + d\alpha\,d\alpha^+$$
$$= -2\kappa(\frac{1}{2}\gamma N + N^2)dt + i(\kappa)^{1/2}N[dW_1(t)+dW_2(t)] \ .$$
$$(2.6)$$

The stochastic noise term $dW_1(t)+dW_2(t)$ is equivalent to a single white noise term $2^{1/2}dW(t)$, and scaling the time as $\tau = 2\kappa t$,

$$dN = -(\frac{1}{2}\gamma N + N^2)d\tau + iN \, dW(\tau) \ . \qquad (2.7)$$

This is a nonlinear complex SDE which can be solved by using a numerical simulation technique. It is also possible to obtain a *linear* equation which describes the time development of the system, and has no instabilities. Thus if we consider the inverse of the intensity, and again use the Ito rules to determine its SDE, we find

$$dv = d\left[\frac{1}{N}\right] = -\frac{1}{N^2}dN + 1/2\frac{2}{N^3}(dN)^2$$

$$= [1 + (\tfrac{1}{2}\gamma - 1)v]d\tau - iv\,dW(\tau) \ . \qquad (2.8)$$

This is an inhomogeneous linear SDE and hence has an exact stochastic solution which will be looked at in more depth in Sec. IV D. Qualitatively (2.8) appears to be a good equation from which to obtain information about N. Problems can only occur at the origin which corresponds to the intensity becoming unbounded. However, since this phase-space point is nonattracting, that is $dv \approx d\tau$ near $v = 0$, any trajectory close to the origin will tend to drift past without actually reaching it. There will, of course, be trajectories which pass through the origin, but the relative probability of any of these is clearly of measure zero.

Finally the equations for the α and α^+ may be best simulated by taking the natural logarithm of the variables, that is,

$$dx = d(\ln\alpha) = \frac{1}{\alpha}d\alpha - \frac{1}{2\alpha^2}(d\alpha)^2$$

$$= \kappa[\tfrac{1}{2}(1 - \gamma) - N]dt + i(\kappa)^{1/2}dW_1(t) \ , \quad (2.9)$$

$$dy = d(\ln\alpha^+) = \kappa[\tfrac{1}{2}(1 - \gamma) - N]dt + i(\kappa)^{1/2}dW_2(t) \ .$$

$$(2.10)$$

The effect of the quantum noise can thus be seen to cause a random complex part in x and y which breaks down the classical conjugacy between the cavity-field variables. The stability of (2.9) and (2.10) is then determined solely by the stability properties of the intensity equation.

III. METHODS OF NUMERICAL SIMULATION

A. Introduction

A general set of stochastic differential equations is now considered, having the form

$$\underline{dx} = \underline{A}(\underline{x})dt + \mathbf{B}(\underline{x})\cdot\underline{dW}(t) \ . \qquad (3.1)$$

These will be either Ito or Stratonovich equations, depending on their method of derivation. However, using the transformations described in Gardiner,[7] both Ito and Stratonovich integration schemes may be employed to solve (3.1) in all cases.

The simplest scheme for the simulation of the Ito SDE is the Euler algorithm which replaces (3.1) with a set of coupled difference equations,

$$\underline{\Delta x}^n = \underline{x}^{n+1} - \underline{x}^n = \underline{A}(\underline{x}^n)\Delta t + \mathbf{B}(\underline{x}^n)\cdot\underline{\Delta W}^n \ , \qquad (3.2)$$

where the stochastic part $\underline{\Delta W}$ is calculated at each time step by

$$\underline{\Delta W}^n = \underline{Z}(n)(\Delta t)^{1/2} \ , \qquad (3.3)$$

$\underline{Z}(n)$ being a vector of independent pseudorandom numbers from the distribution $N(0,1)$. The Euler method, however, has poor stability properties and so often requires the use of impractically small time steps.

B. Improved methods of numerical simulation

A major improvement in the method is to adopt the mixed explicit-implicit scheme of McNeil and Craig[4] for the integration of Ito SDE's. This involves treating the deterministic part implicitly via

$$\underline{\Delta x}^n = \underline{A}(\underline{x}^{n+\theta_1})\Delta t + \mathbf{B}(\underline{x}^n)\cdot\underline{\Delta W}^n, \quad \theta_1 \in [0,1] \ . \quad (3.4)$$

By performing a stability analysis on the deterministic equation only, McNeil and Craig have shown that for $\theta_1 \geq \tfrac{1}{2}$ the method is "A stable," that is, no restriction exists on the size of the time step in order to obtain stable solutions. We now linearize the deterministic part of (3.4) about the point $\underline{x}^n$ as

$$\underline{A}(\underline{x}^{n+\theta_1}) = \underline{A}(\underline{x}^n) + \mathbf{J}_A^n \cdot \theta_1\underline{\Delta x}^n \ ,$$

$$(\mathbf{J}_A^n)_{ij} = \left[\frac{\partial A_i}{\partial x_j}\right]_{x=x^n} \ , \qquad (3.5)$$

where $\mathbf{J}_A^n$ is the Jacobian of A evaluated at $\underline{x} = \underline{x}^n$. After the substitution of (3.5) into (3.4) we obtain the Ito differential scheme

$$\underline{\Delta x}^n = (1 - \theta_1\mathbf{J}_A^n\Delta t)^{-1}[\underline{A}(\underline{x}^n)\Delta t + \mathbf{B}(\underline{x}^n)\cdot\underline{\Delta W}^n] \ . \qquad (3.6)$$

The choice $\theta_1 = 0$ corresponds to Euler's method. However, for $\theta_1 \geq \tfrac{1}{2}$, we would now expect the method to have considerably improved global stability properties. The choice $\theta_1 = \tfrac{1}{2}$ leads to the "time-centered" algorithm, as it has formally a local error of $(\Delta t)^3$ in the deterministic part.

C. Implicit stochastic methods

A natural extension to the method in Sec. III B, when dealing with stochastic differential equations, would be to also handle the stochastic part implicitly,

$$\underline{\Delta x}^n = \underline{A}(\underline{x}^{n+\theta_1})\Delta t + \mathbf{B}(\underline{x}^{n+\theta_2})\cdot\underline{\Delta W}^n \ ,$$

$$\theta_1, \theta_2 \in [0,1] \qquad (3.7)$$

$$\mathbf{B}(\underline{x}^{n+\theta_2}) = \mathbf{B}(\underline{x}^n) + \mathbf{J}_B^n \cdot \theta_2\underline{\Delta x}^n \ . \qquad (3.8)$$

$\mathbf{J}_B^n$ is now the Jacobian of $\mathbf{B}$ evaluated at $\underline{x} = \underline{x}^n$. The insertion of (3.8) and (3.5) into (3.7) gives rise to the fully implicit integration scheme

$$\underline{\Delta x}^n = (1 - \theta_1\Delta t\mathbf{J}_A^n - \theta_2\mathbf{J}_B^n\cdot\underline{\Delta W}^n)^{-1}$$

$$\times [\underline{A}(\underline{x}^n)\Delta t + \mathbf{B}(\underline{x}^n)\cdot\underline{\Delta W}^n] \ . \qquad (3.9)$$

If we now use a generalized binomial theorem to expand out the inverse in (3.9), then we obtain

$$\underline{\Delta x}^n = \underline{A}(\underline{x}^n)\Delta t + \mathbf{B}(\underline{x}^n)\cdot\underline{\Delta W}^n + \theta_2\mathbf{J}_B^n\cdot\underline{\Delta W}^n\underline{\Delta W}^n + O(\Delta t^{3/2}).$$

$$(3.10)$$

Since $\Delta W^2 = O(\Delta t)$, this means that for $\theta_2 > 0$ the numerical scheme is *no longer* simulating an Ito stochastic differential equation. In fact, the form of the scheme resembles a Stratonovich equation, and will exactly integrate the Stratonovich form of (3.1) with the choice

$\theta_2 = \frac{1}{2}$. This indicates that care needs to be taken with numerical schemes which treat the stochastic part implicitly.

In our applications (3.1) is explicitly an Ito SDE, so that in order to use a fully implicit scheme a correction term is required. However, this can always be found by generalizing the transformations in Gardiner,[7] and involves the replacements

$$\underline{A} = \underline{A}^{(i)} - \theta_2 \mathbf{J_B} \cdot\cdot \mathbf{B}^{(i)}(\underline{x}^n) ,$$
$$\mathbf{B} = \mathbf{B}^{(i)} . \tag{3.11}$$

Substituting these corrections into (3.9) gives the fully implicit algorithm

$$\underline{\Delta x}^n = \left[1 - \theta_1 \Delta t \mathbf{J}_A^n - \theta_2 \mathbf{J_B}^n \cdot \underline{\Delta W}^n + \theta_1 \theta_2 \frac{\partial}{\partial \underline{x}} [\mathbf{J_B}^n \cdot\cdot \mathbf{B}(\underline{x}^n)] \Delta t \right]^{-1}$$
$$\times \{ [\underline{A}(\underline{x}^n) - \theta_2 \mathbf{J_B}^n \cdot\cdot \mathbf{B}(\underline{x}^n)] \Delta t + \mathbf{B}(\underline{x}^n) \cdot \underline{\Delta W}^n \} , \tag{3.12}$$

where all terms now obey Ito statistics.

D. Accuracy of the methods

To analyze the local errors in each integration scheme we use the same procedure as Klauder and Petersen[3] and obtain the exact solution for $\underline{\Delta x}^n$ by Picard's successive approximation method,

$$\underline{\Delta x}^n = \int_{t^n}^{t^n + \Delta t} [\underline{A}(\underline{x}(t)) dt + \mathbf{B}(\underline{x}(t)) \cdot \underline{dW}(t)] \tag{3.13}$$
$$= \int_0^{\Delta t} [\underline{A}(\underline{x}(t^n + \tau)) d\tau + \mathbf{B}(\underline{x}(t^n + \tau)) \cdot \underline{dW}(t^n + \tau)] . \tag{3.14}$$

We now expand $\underline{A}$ and $\mathbf{B}$ in a Taylor series about $\underline{x}(t^n)$,

$$\underline{A}(x(t^n + \tau)) = \underline{A}(\underline{x}^n) + \mathbf{J}_A^n \cdot \underline{\Delta x}^{n,\tau}$$
$$+ \frac{1}{2} \frac{\partial^2 A}{\partial \underline{x}^2} \cdot\cdot (\underline{\Delta x}^{n,\tau})^2 + \cdots , \tag{3.15}$$

$$B(\underline{x}(t^n + \tau)) = \mathbf{B}(\underline{x}^n) + \mathbf{J_B}^n \cdot \underline{\Delta x}^{n,\tau} + \frac{1}{2} \frac{\partial^2 \mathbf{B}}{\partial \underline{x}^2} \cdot\cdot (\underline{\Delta x}^{n,\tau})^2 + \cdots ,$$

where

$$\underline{\Delta x}^{n,\tau} = \underline{x}(t^n + \tau) - \underline{x}(t^n)$$
$$= \int_0^\tau [\underline{A}(\underline{x}(t^n + \tau')) d\tau' + \mathbf{B}(\underline{x}(t^n + \tau')) \cdot \underline{dW}(t^n + \tau')] . \tag{3.16}$$

The lowest-order approximation is to drop all but the first terms in (3.15), substitute into (3.14), and calculate the integrals according to the Ito rules. Extensions may obviously be made to any order in Δt by repeating the process of Taylor expansion, now in (3.16), and retaining terms of higher order in (3.15). To $O(\Delta t^{3/2})$ we obtain

$$\underline{\Delta x}^n = \underline{A}(\underline{x}^n) \Delta t + \mathbf{B}(\underline{x}^n) \cdot \underline{\Delta W} + \mathbf{J}_B^n \cdot \mathbf{B}(\underline{x}^n) \cdot \int_0^{\Delta t} \underline{dW}(t^n + \tau) \int_0^\tau \underline{dW}(t^n + \tau') + \mathbf{J}_A^n \cdot \mathbf{B}(\underline{x}^n) \cdot \int_0^{\Delta t} d\tau \int_0^\tau \underline{dW}(t^n + \tau')$$
$$+ \mathbf{J}_B^n \cdot \underline{A}(\underline{x}^n) \cdot \int_0^{\Delta t} \tau \underline{dW}(t^n + \tau) + (\mathbf{J}_B^n)^2 \cdot\cdot \mathbf{B}(\underline{x}^n) \int_0^{\Delta t} \int_0^\tau \int_0^{\tau'} \underline{dW}(t^n + \tau) \underline{dW}(t^n + \tau') \underline{dW}(t^n + \tau'')$$
$$+ \frac{1}{2} \left[\frac{\partial^2 \mathbf{B}}{\partial \underline{x}^2} \right] \cdot\cdot \mathbf{B}(\underline{x}^n) \mathbf{B}(\underline{x}^n) \int_0^{\Delta t} \int_0^\tau \int_0^\tau \underline{dW}(t^n + \tau) \underline{dW}(t^n + \tau') \underline{dW}(t^n + \tau'') + O(\Delta t^2) . \tag{3.17}$$

In the mean only the first term will contribute, since the third term vanishes owing to the nonanticipating nature of the integrand, and all other terms have an odd number of Wiener increments. That is,

$$\langle \underline{\Delta x}^n \rangle = \underline{A}(\underline{x}^n) \Delta t + O(\Delta t^2) . \tag{3.18}$$

So to analyze the local errors in our numerical schemes, we look at the order of the mean-square difference between the exact solution and each of our algorithms $\langle (\Delta x^n - \Delta u^n)^2 \rangle$. For simplicity we consider the one-dimensional case, where Δx^n is given by (3.17), and Δu^n is the difference equation for each of our numerical schemes.

(i) *Euler method.* From (3.2) we have

$$\Delta u^n = A(x^n) \Delta t + B(x^n) \Delta W \tag{3.19}$$

so that in the mean, $\langle \Delta x^n \rangle = \langle \Delta u^n \rangle$ to $O(\Delta t^{3/2})$. Performing the mean-square analysis, the leading-order term is

$$\langle (\Delta x^n - \Delta u^n)^2 \rangle = [J_B^n B(x^n)]^2 \left\langle \left[\int_0^{\Delta t} dW(t^n + \tau) \int_0^\tau dW(t^n + \tau') \right]^2 \right\rangle = \frac{1}{2} [J_B^n B(x^n)]^2 \Delta t^2 . \tag{3.20}$$

Hence the local error in the Euler method is of $O(\Delta t^2)$.

(ii) *Mixed implicit-explicit method.* We now have Δu^n given by (3.6), and providing the condition

$$|\theta_1 J_A^n \Delta t| < 1 \tag{3.21}$$

is maintained, we may expand the inverse out in a binomial series to obtain

$$\Delta u^n = A(x^n) \Delta t + B(x^n) \Delta W + \theta_1 J_A^n B(x^n) \Delta W \Delta t + \theta_1 J_A^n A(x^n) \Delta t^2 + \cdots . \tag{3.22}$$

In the mean we still have $\langle \Delta x^n \rangle = \langle \Delta u^n \rangle$ to $O(\Delta t^{3/2})$. Equation (3.20) will also provide the leading-order mean-square term, so that the local error in the mixed implicit-explicit method is of $O(\Delta t^2)$, i.e., exactly the same as in the Euler method. However, the global accuracy is governed more by the stability, so that in practice, this is expected to be a

much better method.

(iii) *Fully implicit method.* The fully implicit method is given by (3.12). Again, a condition similar to (3.21) is required to expand the inverse, and finally results in

$$
\Delta u^n = A(x^n)\Delta t + \theta_2 J_B^n B(x^n)(\Delta W^2 - \Delta t) + B(x^n)\Delta W
$$
$$
+ \left[\theta_1 J_A^n B(x^n) + \theta_2 J_B^n A(x^n) - \theta_1\theta_2 \left[\frac{\partial^2 B}{\partial x^2}[B(x^n)]^2 + (J_B^n)^2 B(x^n) \right] \right] \Delta W \, \Delta t
$$
$$
+ \theta_2^2 (J_B^n)^2 B(x^n)(\Delta W^2 - \Delta t)\Delta W + O(\Delta t^2) .
\tag{3.23}
$$

First, since $\langle \Delta W^2 \rangle = \Delta t$, in the mean the fully implicit algorithm will now correctly simulate the Ito SDE to $O(\Delta t^{3/2})$. Performing once more the mean-square analysis

$$
\langle (\Delta x^n - \Delta u^n)^2 \rangle = \left\langle \left[J_B^n B(x^n) \left[\int_0^{\Delta t} dW(t^n+\tau) \int_0^\tau dW(t^n+\tau') - \theta_2(\Delta W^2 - \Delta t) \right] + O(\Delta W \, \Delta t) \right]^2 \right\rangle ,
\tag{3.24}
$$

then it may be shown that, for $\theta_2 = \frac{1}{2}$, the term of $O(\Delta t)^2$ vanishes. There is, thus, an improvement in local accuracy with the fully implicit method. Terms at $O(\Delta t^{5/2})$ are always zero, owing to their having an odd number of stochastic increments. So when we look at the next-order mean-square terms, now at $O(\Delta t^3)$, this then involves the calculation of terms such as

$$
[J_A^n A(x^n)]^2 \left\langle \left[\int_0^{\Delta t} \tau dW(t^n+\tau) - \theta_1\Delta t \, \Delta W \right]^2 \right\rangle .
\tag{3.25}
$$

However, it now proves impossible to reduce this error to zero for any value of θ_1, although a minimum is reached for $\theta_1 = \frac{1}{2}$. Similar results can be shown for the other third-order mean-square terms arising from (3.17). Thus the local error in this method is of $O(\Delta t^3)$.

This is in agreement with the result of Rumelin,[8] that no integration scheme may be constructed that has a local error better than $O(\Delta t^3)$ in the mean square. The best that may be achieved is by using the fully implicit method with the choice of parameters $\theta_1 = \frac{1}{2}$ and $\theta_2 = \frac{1}{2}$, which can be shown to minimize all the third-order terms such as (3.24).

This analysis would then seem to indicate that there is an improvement to be found in local accuracy through the use of the fully implicit method. However, the question remains as to whether these improvements would be apparent when conducting the simulations, as there is no theoretical treatment which can predict the stability of a scheme which treats the stochastic part implicitly.

The double dot notation is defined by setting

$$
(\mathbf{J_B})_{k,l,m} = \frac{\partial B_{k,l}}{\partial x_m}
$$

and

$$
(\mathbf{J_B} \cdot\cdot \mathbf{B})_k = \sum_{l,m} (\mathbf{J_B})_{k,l,m} B_{l,m} .
$$

IV. SIMULATION RESULTS

Simulations were now conducted of the equations developed in Sec. II for a wide range of γ values, and using all the integration schemes obtained in Sec. III. In each case a suitable initial point in phase space is selected, and then the individual trajectories are integrated from 0 to a specified t. In the limit of a large number of trials the ensemble average at each time step represents the time development of the stochastic variable.

As a first step, a comparison was made between the various integration schemes for the $\gamma = 0$ equations. A check was made initially that all methods converged in the ensemble average to the same stationary state, and a cutoff was devised to give an indication of when an individual trajectory diverged (i.e., a numeric spike). It proved most convenient to use the cutoff required in the binomial expansions of methods (ii) and (iii), and since for the N SDE the Jacobian of the drift vector A is of $O(x)$, we define a divergent trajectory as one where

$$
|x_i| \geq \frac{1}{\theta_1 \Delta t}
\tag{4.1}
$$

for any phase-space variable x_i. This definition is then extended to define a cutoff for the Euler algorithm. Now using method (ii) with $\theta_1 = \frac{1}{2}$, and method (iii) with $\theta_1,\theta_2 = \frac{1}{2}$, over a large range of time steps Δt, we obtain Table I.

As expected the v simulation, being linear, was totally stable for all methods and integration steps, there being no spikes with any method, and for any time step. The N simulation results confirm clearly that the Euler algorithm is only reliable for small integration steps. However, it should be noted that even with the A-stable mixed implicit-explicit method (ii) there were still a finite number of spikes. This confirms that for some systems, as we shall see, reasons for these spikes can be intrinsic, rather than simply a poor integration scheme. The results are not conclusive for a comparison between methods (ii) and (iii), although it does appear as if there is no major improvement to be made in the extra linearization of the stochastic terms, while it is definitely more complicated

TABLE I. Entries are the number of divergent spikes found until 2000 nondivergent trajectories are reached.

Δt	N simulation Method (i)	(ii)	(iii)
0.005	12	5	5
0.01	33	6	18
0.05	276	21	42
0.1	984	127	108

computationally. This would suggest that the properties of stability and global accuracy are more important in determining the accuracy of the simulations, rather than the local order of the method.

Finally the Runge-Kutta algorithm of Klauder and Petersen was implemented. This, however, offered no improvement in terms of the number of spikes encountered or in the description of the convergence to the stochastic steady state. Thus for our system of equations, all of these improved stochastic algorithms are seen to be essentially equivalent. For the rest of this paper, then, we shall use the time-centered mixed implicit-explicit method to integrate our stochastic equations.

A. Results of the $\gamma = 0$ simulation

This corresponds to the situation where the cavity mode is only damped nonlinearly, i.e., through two-photon absorption. Then the stochastic limit of the N and v equations was found to be

$$N = \begin{bmatrix} N_x \\ N_y \end{bmatrix} \rightarrow \begin{bmatrix} \frac{1}{2} \\ 0 \end{bmatrix}, \quad v = \begin{bmatrix} v_x \\ v_y \end{bmatrix} \rightarrow \begin{bmatrix} 1 \\ 0 \end{bmatrix} . \tag{4.2}$$

As required the variables N_y and v_y representing the extra dimensions of the positive P representation are zero in the ensemble average. The result $N \rightarrow \frac{1}{2}$ also has a simple physical interpretation, representing a superposition of the stable $|0\rangle$ and $|1\rangle$ number states. An initial coherent state is a Poisson distribution of odd and even number states so that a steady state of $N = \frac{1}{2}$ corresponds to a balanced superposition of final number states.

Now at each time step, and for each trajectory we have the relation between N and v

$$N_x = \frac{v_x}{v_x^2 + v_y^2}, \quad N_y = \frac{-v_y}{y_x^2 + v_y^2} . \tag{4.3}$$

However, since

$$\langle N_x[\infty] \rangle = \frac{1}{2} \neq \frac{\langle v_x[\infty] \rangle}{\langle v_x[\infty] \rangle^2 + \langle v_y[\infty] \rangle^2} , \tag{4.4}$$

there is no simple way to relate the stochastic limits of the numerically stable v equation with the physically interesting N equation. Instead, when simulating the v equation for each trajectory, at each time step it is necessary to calculate N_x and N_y from (4.3), and then ensemble average N_x and N_y over all the v trajectories. We shall refer to this process of simulating the v trajectories and using them to generate the time behavior of N as the $1/v$ simulation.

With this refinement the N and $1/v$ simulations give rise to the same stochastic time development and stationary state (see Fig. 1). This would seem to confirm that our N equation, although nonlinear, is being simulated correctly.

It was noted above that with all methods there was a finite number of spikes in the N simulation. The existence of these spikes has been of some concern recently.[9] Because of the simplicity of our equations we are able to isolate the cause of these spikes and understand better their purpose in the positive P simulations. This can be seen when we consider the pair of deterministic equations
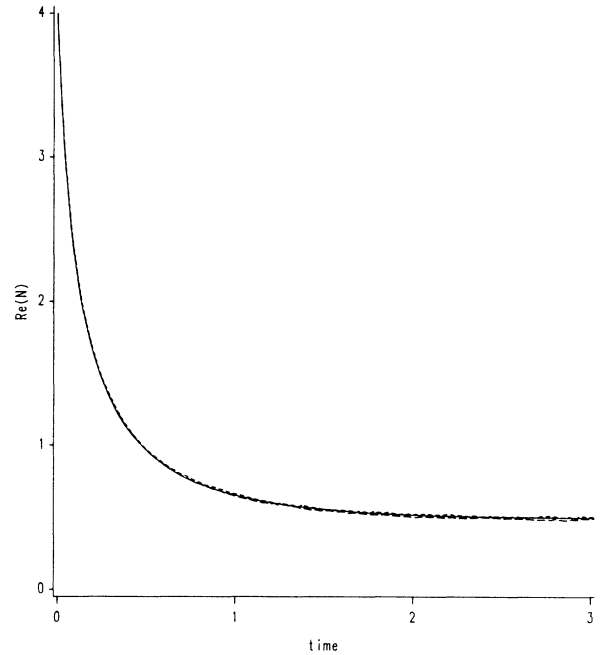

FIG. 1. Ensemble average of cavity intensity Re(N) vs time, $\gamma = 0$. ——, jump process, 200 000 trials; -----, $1/v$ simulation, 15 000 trials; — — —, N simulation, 15 000 trials. Parameters: $dt = 0.01$, $\gamma = 0$.

resulting from (2.7),

$$dN_x = -(N_x^2 - N_y^2)d\tau, \quad dN_y = -2N_xN_yd\tau , \tag{4.5}$$

then if $N = (-X, 0)$ for any $X > 0$,

$$dN_x = -X^2 d\tau, \quad dN_y = 0, \quad N \rightarrow (-\infty, 0) . $$

That is, the equation is unstable for an initial condition on the negative real axis. Of course N being on the negative real axis corresponds to an unphysical situation, and in the deterministic analysis starting from a physical initial condition could never be reached. However, if we now consider the addition of the stochastic parts

$$dN_x = -(N_x^2 - N_y^2)d\tau - N_y dW(\tau) ,$$
$$dN_y = -2N_xN_y d\tau + N_x dW(\tau) , \tag{4.6}$$

then the effect of the noise terms can lead to a single trajectory landing on the negative real axis. There will then be an explosion along the negative real axis as in the deterministic case, but owing to the coupling $N_x dW(\tau)$, N_y must also go away from zero. The deterministic part of the N_y equation then takes over and causes N_y to quickly increase in the direction of the initial sign of N_y. There is, thus, a dramatic shooting out into the nonclassical complex phase space. Eventually the N_y^2 term in the deterministic part of the N_x equation will stifle the unstable N_x^2 term causing N_x to return to the origin and become positive. But for N_x positive, the deterministic part of the N_y equation reverses sign, so that N_y will now tend back to zero. As this happens, N_x^2 will again dominate over N_y^2 causing N_x to stop increasing, and to return towards small positive values. We are now back in the "physical subspace" of N_x positive and N_y small. The complete description of this spike is of a large loop in the
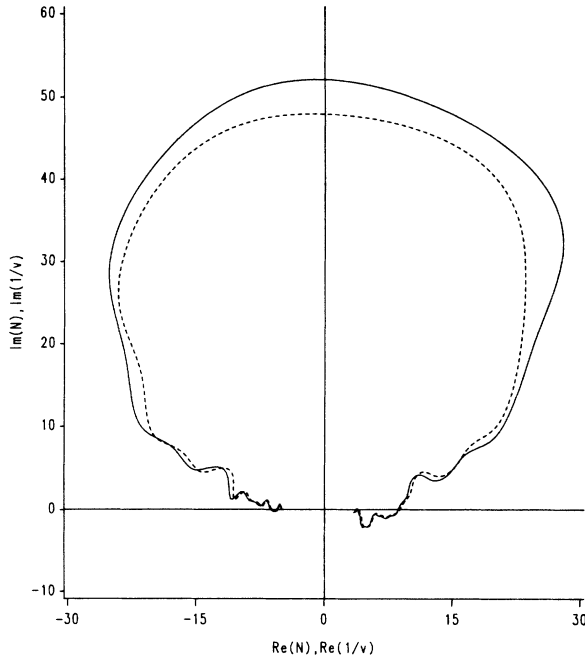
FIG. 2. Single-trajectory complex plot showing spike; ———, N simulation; -----, $1/v$ simulation. Parameters; $dt=0.02$, $\gamma=0$, X (initial condition) $=-5$, $t_{\max}=0.5$.

extended phase space which is almost symmetric about the N_y axis and is randomly a loop in the upper or lower half plane (see Fig. 2). The quantum noise affects the trajectory in two ways, firstly allowing it to explore the extended phase space, but then providing this looping mechanism to return it to the physical domain. The exact size of the loop is not constant and depends on the values of the random noise terms, but it is clear that the loop must be of a finite size and eventually return close to the positive real axis. It is only during this time that there is any significant excursion into the extra dimensions of the positive P representation.

This explanation of the spikes supports the notion of Carmichael et al.,[10] that there is no physical basis for these spikes. Indeed it may be seen that as the loop is approximately symmetric about the imaginary axis, and equally likely to shoot out in the positive or negative imaginary direction, then in the ensemble average it produces no physical contribution. However, due to the finite ensembles that we are using, these spikes will result in fluctuations about the physical development.

In the N simulation, all methods become inaccurate on the spike trajectories, so it is necessary to retain a cutoff and remove from the ensemble average all trajectories exceeding this. In the v simulation, spikes correspond to the trajectory tending close to the origin, and since everything is well behaved here, the trajectory may be followed accurately and no cutoff is required. In general, to avoid the unsatisfactory practice of just ignoring spike trajectories, we would suggest the best procedure is to establish a changeover sphere in phase space for the variable being integrated. If a trajectory goes beyond this boundary, a switch is then made and the inverse variable equation is

used to track the trajectory until it returns inside the sphere and the variable equation is restarted.

B. Results of the $\gamma > 0$ simulation

We now extend the simulations to include a mechanism for linear damping. The time development for the intensity N is obtained by performing the N and $1/v$ simulations using method (ii). As can be seen in Figs. 3 and 4 a definite stochastic limit is reached in both situations where

$$N \rightarrow \tfrac{1}{2}(1-\gamma) \text{ for } \gamma < 1, \quad N \rightarrow 0 \text{ for } \gamma \geq 1 .$$

However, this result is in conflict with our physical interpretation. We would have expected that as soon as a linear damping mechanism was introduced, even with a small damping rate compared to the nonlinear mechanism, that the $|1\rangle$ state would no longer be absolutely stable due to a finite possibility of a transition to the ground state. Thus we would expect $N \rightarrow 0$ for all $\gamma > 0$, with the decay curve steepening for larger γ.

To test the time scale for this decay we went back to the master equation (2.2), and defining $P(n)=\langle n|\rho|n\rangle$, the diagonal matrix element in the number-state representation, we obtained the equation

$$\dot{P}(n)=\kappa[(n+1)(n+2)P(n+2)+\gamma(n+1)P(n+1)$$
$$-n(n-1+\gamma)P(n)] . \qquad (4.7)$$

This is the equation of a unidirectional jump process, with a transition rate per unit time from a state $|n\rangle$ given by
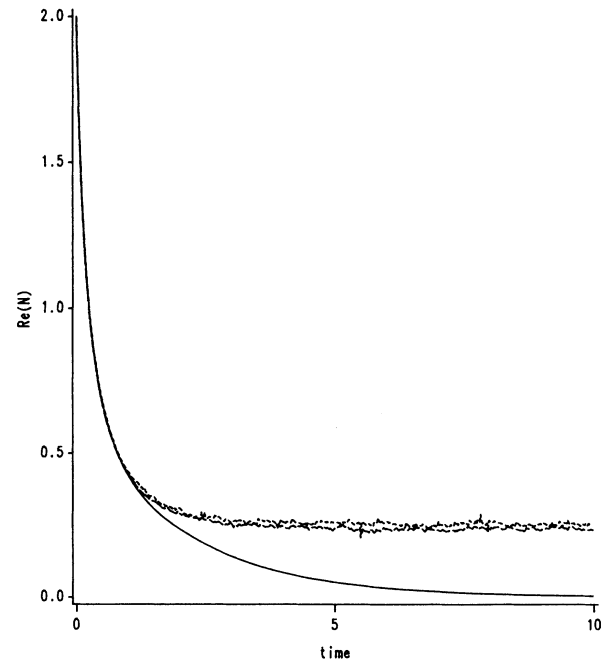
$$\lambda=\kappa n(n-1+\gamma) , \qquad (4.8)$$

FIG. 3. Ensemble average of cavity intensity Re(N) vs time, $\gamma=0.5$. ———, jump process, 200 000 trials; -----, $1/v$ simulation, 15 000 trials; — — —, N simulation, 15 000 trials. Parameters: $dt=0.02$, $\gamma=0.5$.
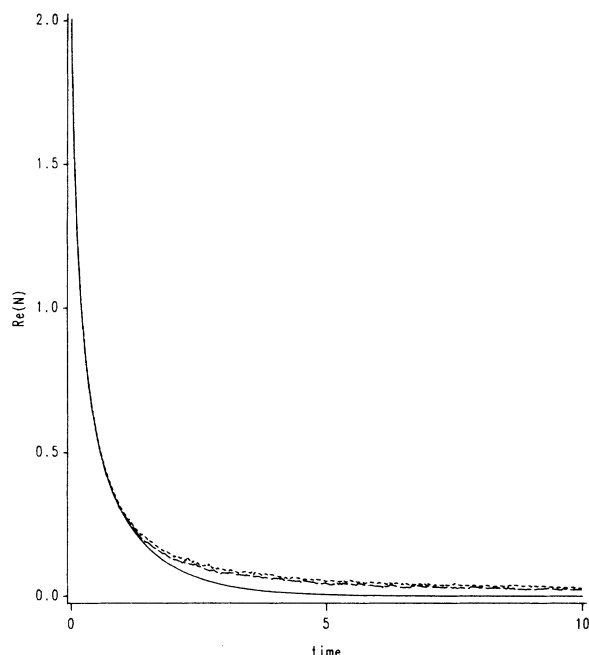
FIG. 4. Ensemble average of cavity intensity $Re(N)$ vs time, $\gamma=1$. ———, jump process, 200 000 trials; -----, $1/v$ simulation, 15 000 trials; — — —, N simulation, 15 000 trials. Parameters; $dt=0.02$, $\gamma=1$.

made up of two transitions: $n \rightarrow n-2$, $n \rightarrow n-1$, with transition rates $\lambda_{nl}=\kappa n(n-1)$ and $\lambda_l=\kappa\gamma n$.

The simulation of a jump process is a well-studied procedure; to correspond with the phase-space simulation we scale the time as $\tau=2\kappa t$, and note that an initial condition in the N simulation of X (real) is equivalent to a Poissonian distribution of mean X for the starting values of the jump process.

For $\gamma=0$, λ has two stationary values at $n=0,1$ so that the time development of the ensemble average of the intensity n is towards the ratio of the final number of $|1\rangle$ states to $|0\rangle$ states. As seen in Fig. 1, for large initial conditions X this ratio is $\approx\frac{1}{2}$ and the simulations of the positive P and jump process give rise to identical time development, within the accuracy of the simulations. Due to the Poissonian probability distribution for smaller initial conditions, the final ground state will dominate, resulting in a result of less than half for the stationary state of the jump process [i.e., for $X=0.5$ n(jump)$\rightarrow$0.316]. However, in the positive P simulations, the intensity variable still tends strictly towards half, now at variance with our physical predictions.

For $\gamma>0$, the only stationary value of λ is at $n=0$ (since $n\in W$), and hence the ensemble average $n(t)\rightarrow0$ as $t\rightarrow\infty$. This is in direct contradiction with our previous simulation results (Figs. 3 and 4), although in accordance with our physical expectations. We notice from (4.8) that there is a second stationary state given by $n=1-\gamma$, $0\leq\gamma\leq1$, and a superposition of this and the ground state would give rise to the $N\rightarrow\frac{1}{2}(1-\gamma)$ stochastic limit of the simulations. However, there is no physi-

cal reason for the fractional photon number states that this explanation would require.

C. Simulation of the field variables

In the next simulation, our stochastic equations were used to obtain the time development of the α and α^+ variables. Using the results of Sec. II we integrated

$$dx(\tau)=[\tfrac{1}{2}(1-\gamma)-N(\tau)]d\tau+i\,dW_1(\tau)\,,\qquad(4.9)$$

where $N(\tau)$ is found at each time step by integrating

$$dN=-2(\tfrac{1}{2}\gamma N+N^2)d\tau+i2^{1/2}[dW_1(\tau)+dW_2(\tau)]$$

$$(4.10)$$

or equivalently using the $1/v$ simulation. For each trajectory we calculated $\alpha(\tau)=\exp[x(\tau)]$ and found its ensemble average over all the trajectories at each time step. The time development of α^+ may be similarly determined using the equation for y or the relation $\alpha^+=N/\alpha$. The results for all γ show that α and α^+ decay to zero (see Fig. 5) in the stochastic limit. The stability properties of the x and y variables are totally determined by the stability properties of N, and hence do exhibit spikes, although scaled by Δt.

It is most interesting here to look at the time development of α and N for a single trajectory [Figs. 6(a) and 6(b)]. We see here that α (and α^+ similarly) tends towards a circular distribution about the origin. The radius of the circle is determined by γ, being a maximum for $\gamma=0$ and zero for $\gamma\geq1$. The trajectory of the intensity variable N, however, is a crescent, located predominantly
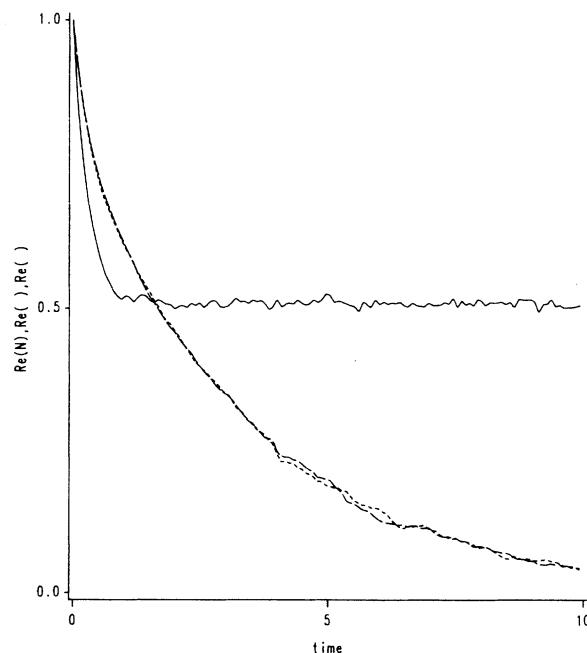

FIG. 5. Ensemble average of cavity and field variables in time, $\gamma=0$. ———, N obtained by $1/v$ simulation; -----, α obtained by x simulation; — — —, α^+ obtained from N/α. Parameters: 10 000 trials, $dt=0.02$, $\gamma=0$.
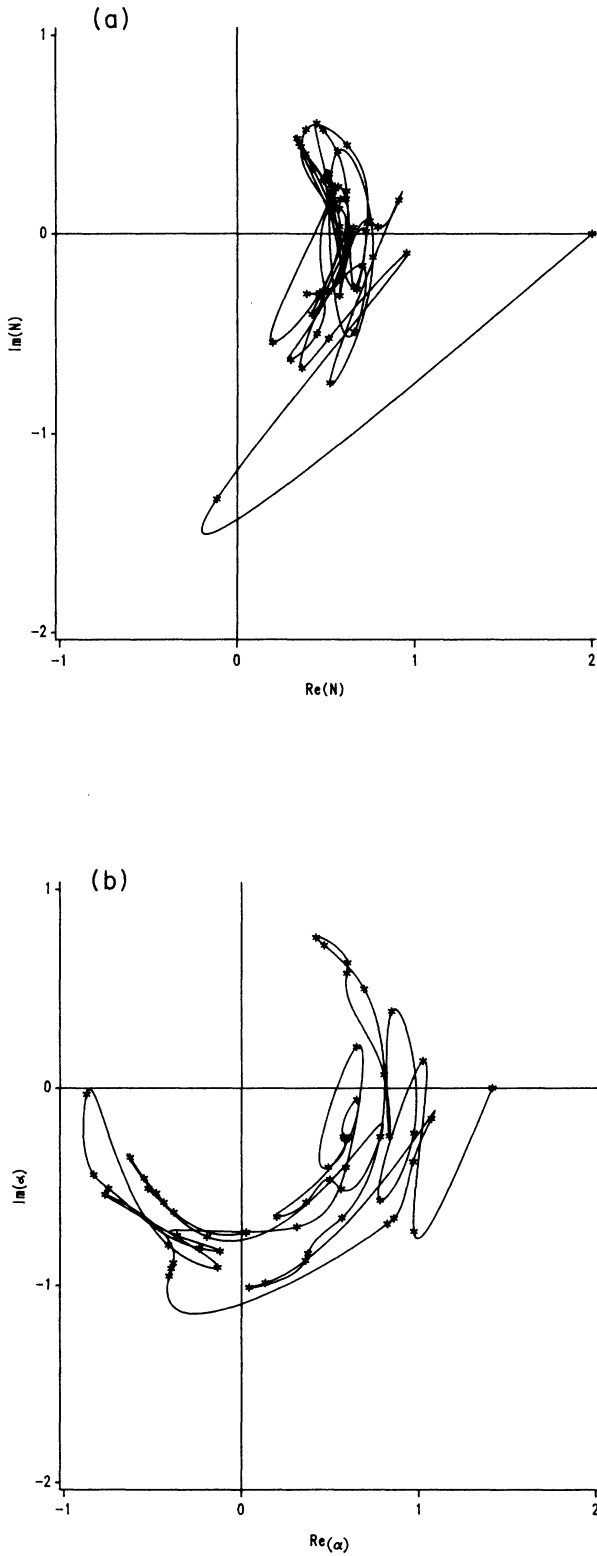
FIG. 6. (a) Single-trajectory complex plot of N in time. $*$, N obtained by $1/v$ simulation, every fourth time step. Parameters: $dt=0.01$, $\gamma=0$, X (initial condition)$=2$, $t_{max}=20$. (b) Single-trajectory complex plot of α in time. $*$, α obtained by x simulation, every fourth time step. Parameters: $dt=0.01$, $\gamma=0$, X (initial condition)$=1.414$, $t_{max}=20$.

in the real positive half plane and symmetric about the real axis. The perfect phase diffusion in the distribution for the field variables explains why the ensemble average of the α and α^+ variables tends to zero in the stochastic steady-state limit while the intensity remains finite.

D. An exact solution for the v equation

In Sec. II we obtained an equation for the variable $1/N$ (2.8), which is a linear inhomogeneous process. To solve this, we considered first the homogeneous process

$$du = [(\tfrac{1}{2}\gamma - 1)dt - i\, dW(t)]u \ . \tag{4.11}$$

Defining then the variable $y = \ln u$, it will have the equation

$$dy = \tfrac{1}{2}(\gamma - 1)dt - i\, dW(t) \ . \tag{4.12}$$

This may be directly integrated, and results in the solution for u,

$$u(t) = u(0)\exp\left[\int_0^t [\tfrac{1}{2}(\gamma - 1)dt' - i\, dW(t')]\right]$$

$$= u(0)\phi(t) \ , \tag{4.13}$$

which defines

$$\phi(t) = e^{(\gamma-1)t/2}\exp\left[-i\int_0^t dW(t')\right] \ . \tag{4.14}$$

So now dealing with the time-scaled inhomogeneous process

$$dv = [1 + (\tfrac{1}{2}\gamma - 1)v]dt - iv\, dW(t) \ . \tag{4.15}$$

If we define $z = v[\phi(t)]^{-1}$, then as is shown by Gardiner[11] for the general case, we obtain the equation for the z variable

$$dz = dt\, [\phi(t)]^{-1} \tag{4.16}$$

and the exact stochastic solution for $v(t)$ is

$$v(t) = v(0)e^{(\gamma-1)t/2}\exp\left[-i\int_0^t dW(t'')\right]$$

$$+ \int_0^t dt'\exp\left[\tfrac{1}{2}(\gamma-1)(t-t')-i\int_{t'}^t dW(t'')\right] \ . \tag{4.17}$$

This solution may be used to find the time development of the mean of $v(t)$. .That is, taking the expectation value of (4.17), together with the rule for any Gaussian variable Z with zero mean,

$$\langle\exp(Z)\rangle = \exp(\tfrac{1}{2}\langle Z^2\rangle) \ , \tag{4.18}$$

then after performing the integration it may be shown that

$$\langle v(t)\rangle = e^{(\gamma-2)t/2}\left[\langle v(0)\rangle - \frac{2}{2-\gamma}\right] + \frac{2}{2-\gamma} \ . \tag{4.19}$$

Hence in the steady-state limit, for $\gamma < 2$,

$$\lim_{n\to\infty}\langle v(t)\rangle \to \frac{2}{2-\gamma} \ ,$$

and for $\gamma \geq 2$

$$\lim_{n \to \infty} \langle v(t) \rangle \to \infty \ . \tag{4.20}$$

The results of the simulations for v conform exactly in the steady state to (4.20), and the time development clearly has the right type of γ-dependent exponential decay. Unfortunately though, it is impossible to analytically relate these exact results for v to the physically interesting N results, other than to show that for $\gamma \geq 2$, N must tend towards zero.

One numerical approach that we can take is to numerically integrate (4.17) by using a routine such as the trapezium rule. The stochastic part is handled in a similar fashion to the simulation as

$$\int_0^t dW(t') \approx \sum_{k=0}^{t/\Delta t} C(\Delta t)^{1/2} \ , \tag{4.21}$$

where C is a pseudorandom number from $N(0,1)$ with an ensemble average taken of $1/v$ at each time step of a large number of integrations. Looking at the results for $\gamma = 0$ and $\frac{1}{2}$ (see Fig. 7), we see that they show exactly the same time development as in the simulations, confirming the correct numerical simulation of our equations.

V. ANALYSIS OF SIMULATION RESULTS

When we look at the results of the simulations conducted in Sec. IV, we see there is a definite anomaly in the behavior of the positive P simulation, when compared with both the jump process results and our physical intuition. This is seen most graphically in the different steady states obtained for certain γ values by the various
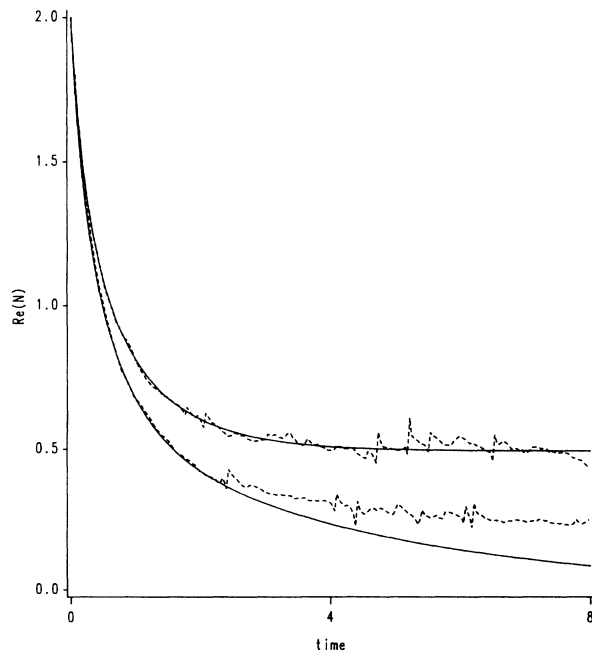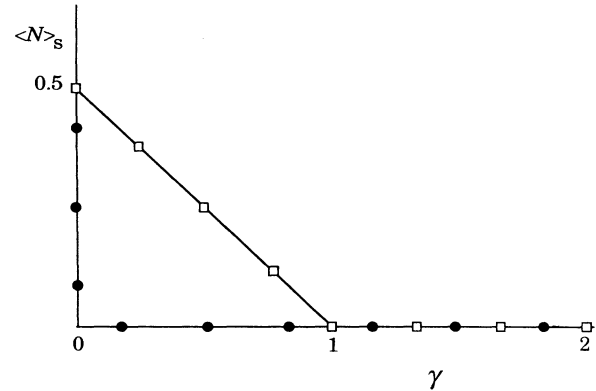
FIG. 8. Diagram of steady-state intensity vs γ. $\square$, N and $1/v$ simulation; $\bullet$, jump process.

methods (Fig. 8). As indicated in the diagram, the significant values of the horizontal axis are at $\gamma = 1$ and 2.

For $\gamma < 1$, there is a discrepancy between the stochastic stationary states (although for $\gamma = 0$ this is only apparent for small initial conditions). Other nonphysical behavior is also observed (Fig. 9) in this region, where the cavity intensity increases uniformly for some time although there is no physical process in the Hamiltonian which permits this. What is noticeable from Fig. 9 is that the simulation always follows initially the correct time development, but then there is suddenly a dramatic change as though some hidden factor in the equations causes the simulations to tend towards a different limit.

For $1 \leq \gamma < 2$ the simulations all now decay to zero, although, as is shown in Fig. 4, there are differences in the moderate t time development when compared with the equivalent jump process. However, as γ increases, the intensity curves for the N, $1/v$, the jump simulations tend to approach each other more closely. The simulations for $\gamma \geq 2$ all decay to zero in numerically indistinguishable fashions by all methods. This is in line with our theoretical v analysis, which showed that for $\gamma \geq 2$ then $v \to \infty$ rapidly, which must force the intensity N to quickly decrease to zero.

There seems no doubt that the simulations are correct, that is, the time development is the one given by the form of the stochastic equations. In this paper we have used straight N simulations, the $1/v$ simulation, and the integration of the exact stochastic v solution—all with identical results. Even though numerical problems such as spikes do occur in some of these techniques, they may be dealt with consistently and without introducing any systematic error. We are thus confident that the explanation for this anomaly is not simply a numerical one.

Another important piece of evidence is that of the jump process simulation, which proceeds directly from the master equation. This was found to conform to our physical predictions for all values of γ, and all initial conditions. This would seem to confirm that our Hamiltonian model does correctly represent the physics of the situation, and that the derivation of the master equation is sound.

This leaves then, the positive P representation itself as the only remaining source of the anomaly. We consider

FIG. 7. Exact $1/v$ integration of cavity intensity vs time; Upper curves: $\gamma = 0$, $dt = 0.02$; ———, equivalent jump process, 100 000 trials; -----, $1/v$ integration, 500 trials. Lower curves: $\gamma = 0.5$, $dt = 0.02$; ———, equivalent jump process, 100 000 trials; -----, $1/v$ integration, 500 trials.
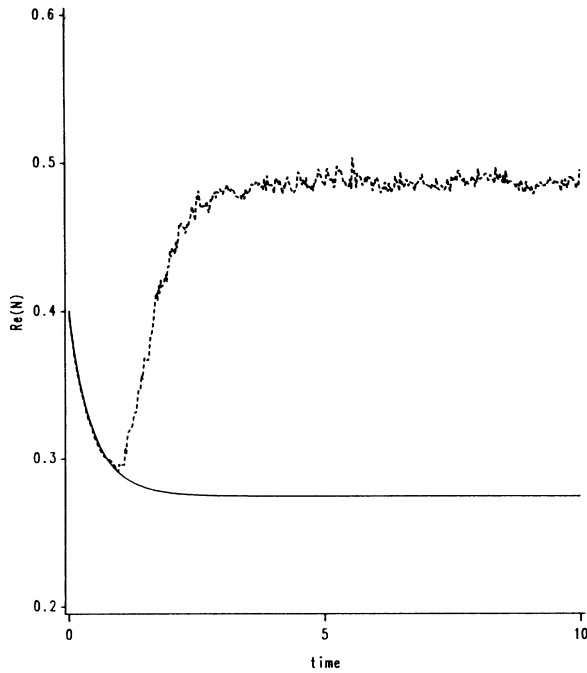
FIG. 9. N simulation of intensity vs time, small initial condition. ———, jump process, 200 000 trials; -----, N simulation, 15 000 trials. Parameters; $dt = 0.02$, $\gamma = 0$.

that this is most likely to be in the assumption of the vanishing of the boundary terms as the phase-space variables tend towards infinity in the extended phase space. In derivations of the positive P representation this step is never explicitly checked, and since the appearance of these terms affects the normalization properties of the solution, their exclusion may explain the nonphysical properties exhibited in our equations. This conjecture is now presented in greater detail in the conclusion to our analysis of simulations in the positive P representation.

VI. CONCLUSION

The positive P representation has been in existence for ten years now, and although there has been some concern expressed about the spiking behavior, we believe that this is the first investigation in which one can say with some confidence that the positive P representation predictions are not correct—they are at variance with what the master equation itself predicts. It is therefore important to understand what is going wrong.

While a conclusive answer cannot be given, a very good indication can be found. Firstly one may notice that the derivation of the positive P Fokker-Planck equation involves a partial integration and the subsequent discarding of surface terms. If we consider, for example, a diagonal coherent-state matrix element $\langle\beta|\rho|\beta\rangle$ of the density operator, when ρ is written as a positive P distribution, we have

$$\langle\beta|\rho|\beta\rangle = \int d^2\alpha \int d^2\alpha^+ \frac{\langle\beta|\alpha\rangle\langle\alpha^+|\beta\rangle}{\langle\alpha^+|\alpha\rangle} P(\alpha,\alpha^+) \qquad (6.1)$$

$$= \int d^2\alpha \int d^2\alpha^+ \exp[-(\beta-\alpha)(\beta-\alpha^+)^*]$$

$$\times P(\alpha,\alpha^+) . \qquad (6.2)$$

Since α and α^+ are allowed to vary all over the complex plane, we can see that the direction in which $\alpha^+ = -\alpha$ is particularly dangerous, since the exponential factor can blow up like $\exp(|\alpha|^2)$. This means we must have

$$P(\alpha,-\alpha) \approx \exp(-|\alpha|^2) \qquad (6.3)$$

at the very least for convergence. The explicit construction of the positive P function (see Gardiner[12] for details)

$$P(\alpha,\alpha^+) = \frac{1}{4\pi^2} \exp[-\tfrac{1}{4}|\alpha-(\alpha^+)^*|^2]$$

$$\times \langle \tfrac{1}{2}[\alpha+(\alpha^+)^*]|\rho|\tfrac{1}{2}[\alpha+(\alpha^+)^*]\rangle \qquad (6.4)$$

can be seen to only just satisfy this constraint for reasonable ρ. However, it must be remembered that the positive P function is not unique, and that the explicit construction merely proves the existence of at least one positive P function. In particular, the solution of the positive P Fokker-Planck equation is certainly not of this kind. In the model being studied here, for $\gamma \leq 2$, there is always a probability of $v(t)$ passing close to the origin in each trajectory; in other words, the probability density of v is nonzero at $v=0$ in the stationary state. Translated into a statement about $P(v)$, and hence $P(\alpha,\alpha^+)$, this means that the probability density $P(\alpha,\alpha^+)$ will go to zero at best like $|\alpha\alpha^+|^{-3}$, which would certainly violate the growth condition (6.3) rather badly. On the other hand, for $\gamma > 2$, $v(t)$ must become infinite as $t \to \infty$, so that the probability density at the origin of v will be zero in the stationary state. In fact, in the stationary state, the v probability is zero everywhere except at $v = \infty$, which certainly satisfies the condition (6.3).

In the time evolving state, it is clear that there is always some probability of going near the origin in the v equation, but from the simulation results, this can only be significant when $\gamma < 2$. Also in the initial time development from a physical initial condition, we would expect there to be an accumulation of probability at the origin of v. This growth in probability for $\gamma < 2$ provides a good explanation of the phenomena noted in Sec. V whereby, for any γ, the simulation initially displays the right time development (see Figs. 3 and 9, for examples). The hidden factor which causes the simulation to go wrong is then intimately related to a finite probability of the v trajectory being at the origin.

We can summarize our conclusions in a conjecture. The spikes always arise from a reciprocal variable passing near the origin, and when this happens the probability density (in the reciprocal variable) at the origin is nonzero. This corresponds to $P(\alpha,\alpha^+) \approx |\alpha\alpha^+|^{-3}$ at infinity, in which case the positive P representation is not valid. Thus if spiking behavior is observed, the results of the simulations are not reliable, although they may accidentally nevertheless be accurate, as appears to be the case for $\gamma = 0$ with large initial conditions (also in the steady-state limit for $l \leq \gamma \leq 2$).

A proof of this conjecture is left to either a later work

or to others. It seems to us to be more important at this stage to analyze what possible correction terms could be implemented to compensate for the spiking, since a method whose usefulness has proved itself so widely should not be abandoned lightly.

ACKNOWLEDGMENTS

APPENDIX: A COMPLEX P REPRESENTATION STEADY-STATE SOLUTION

A generalized P distribution, which may give rise to an analytic steady-state solution under certain conditions, is the complex P representation, where the density operator ρ is given by

$$\rho = \int_C d\alpha \int_{C'} d\alpha^+ P(\alpha, \alpha^+) \frac{|\alpha\rangle\langle(\alpha^+)^*|}{\langle(\alpha^+)^*|\alpha\rangle} , \quad \text{(A1)}$$

C and C' being contours in the complex α and α^+ planes. It is then possible to rederive the Fokker-Planck equation for $P(\alpha, \alpha^+)$ (2.4), and write it in the form of probability currents

$$\frac{\partial}{\partial \tau} P(\alpha, \alpha^+) = \left[\frac{\partial}{\partial \alpha} \left[\alpha^+ \alpha^2 + \frac{1}{2}\gamma\alpha - \frac{1}{2}\frac{\partial}{\partial \alpha}\alpha^2 \right] \right.$$
$$+ \frac{\partial}{\partial \alpha^+} \left[\alpha\alpha^{+2} + \frac{1}{2}\gamma\alpha^+ \right.$$
$$\left. \left. - \frac{1}{2}\frac{\partial}{\partial \alpha^+}\alpha^{+2} \right] \right] P(\alpha, \alpha^+) .$$

$$\text{(A2)}$$

The most general requirements for a steady-state solution are then

$$\left[\alpha^+ \alpha^2 + \frac{1}{2}\gamma\alpha - \frac{1}{2}\frac{\partial}{\partial \alpha}\alpha^2 \right] P_s(\alpha, \alpha^+) = \phi(\alpha^+) , \quad \text{(A3)}$$

$$\left[\alpha\alpha^{+2} + \frac{1}{2}\gamma\alpha^+ - \frac{1}{2}\frac{\partial}{\partial \alpha^+}\alpha^{+2} \right] P_s(\alpha, \alpha^+) = \psi(\alpha) , \quad \text{(A4)}$$

where the $\phi(\alpha^+)$ and $\psi(\alpha)$ must in addition satisfy some generalized potential conditions. To find the form of these functions we write P_s as

$$P_s(\alpha, \alpha^+) = \frac{Q(\alpha, \alpha^+)}{(\alpha\alpha^+)^2} , \quad \text{(A5)}$$

then (A3) and (A4) can be written as

$$\frac{\partial}{\partial \alpha}[e^{-2\alpha\alpha^+}(\alpha\alpha^+)^{-\gamma}Q] = -2\theta(\alpha^+)(\alpha\alpha^+)^{-\gamma}e^{-2\alpha\alpha^+} , \quad \text{(A6)}$$

$$\frac{\partial}{\partial \alpha^+}[e^{-2\alpha\alpha^+}(\alpha\alpha^+)^{-\gamma}Q] = -2\chi(\alpha)(\alpha\alpha^+)^{-\gamma}e^{-2\alpha\alpha^+} , \quad \text{(A7)}$$

where we have defined for simplicity

$$\theta(\alpha^+) = \alpha^{+2}\phi(\alpha^+), \quad \chi(\alpha) = \alpha^2\psi(\alpha) . \quad \text{(A8)}$$

The generalized potential conditions are now see to be

$$\frac{\partial}{\partial \alpha^+} \left[\frac{\partial}{\partial \alpha}[e^{-2\alpha\alpha^-}(\alpha\alpha^+)^{-\gamma}Q] \right]$$
$$= \frac{\partial}{\partial \alpha} \left[\frac{\partial}{\partial \alpha^+}[e^{-2\alpha\alpha^+}(\alpha\alpha^+)^{-\gamma}Q] \right] , \quad \text{(A9)}$$

so we obtain the condition on $\theta(\alpha^+)$ and $\chi(\alpha)$

$$\frac{\partial}{\partial \alpha^+}[-2\theta(\alpha^+)(\alpha\alpha^+)^{-\gamma}e^{-2\alpha\alpha^+}]$$
$$= \frac{\partial}{\partial \alpha}[-2\chi(\alpha)(\alpha\alpha^+)^{-\gamma}e^{-2\alpha\alpha^+}] . \quad \text{(A10)}$$

After some cancellation (A10) becomes

$$\frac{\partial}{\partial \alpha^+}\theta(\alpha^+) - \frac{\gamma\theta(\alpha^+)}{\alpha^+} - 2\alpha\theta(\alpha^+)$$
$$= \frac{\partial}{\partial \alpha}\chi(\alpha) - \frac{\gamma\chi(\alpha)}{\alpha} - 2\alpha^+\chi(\alpha) , \quad \text{(A11)}$$

which can only be satisfied for

$$\theta(\alpha^+) = 0, \quad \chi(\alpha) = 0 ,$$

for the ordinary potential solution, or

$$\theta(\alpha^+) = A\alpha^+, \quad \chi(\alpha) = A\alpha .$$

So taking a linear combination of these, the solution of Q will be given by either

$$\frac{\partial}{\partial \alpha}[(\alpha\alpha^+)^{-\gamma}e^{-2\alpha\alpha^+}Q] = -2A\alpha^+(\alpha\alpha^+)^{-\gamma}e^{-2\alpha\alpha^+} ,$$

$$\text{(A12)}$$

or

$$\frac{\partial}{\partial \alpha^+}[(\alpha\alpha^+)^{-\gamma}e^{-2\alpha\alpha^+}Q] = -2A\alpha(\alpha\alpha^+)^{-\gamma}e^{-2\alpha\alpha^+} .$$

$$\text{(A13)}$$

(i) *Case* $\gamma = 0$. We now perform either of the indefinite integrals (A12) or (A13) to give

$$Q = A + Be^{2\alpha\alpha^+} \quad \text{(A14)}$$

where B is a constant of integration and hence

$$P_s(\alpha, \alpha^+) = A(\alpha\alpha^+)^{-2} + B(\alpha\alpha^+)^{-2}e^{2\alpha\alpha^+} . \quad \text{(A15)}$$

(ii) *Case* $\gamma \geq 0$. We now obtain for Q

$$Q = B(\alpha\alpha^+)^\gamma e^{2\alpha\alpha^+} - 2A(\alpha\alpha^+)^\gamma e^{2\alpha\alpha^+}(\alpha^+)^{-\gamma+1}I ,$$

$$\text{(A16)}$$

where I is the indefinite integral

$$I = \int d\alpha\, \alpha^{-\gamma}e^{-2\alpha\alpha^+} . \quad \text{(A17)}$$

This integral may be calculated using a power-series expansion, and although modifications have to be made at

integral values for γ, by analytic continuation the general steady-state solution is found to be

$$P_s(\alpha,\alpha^+) = B(\alpha\alpha^+)^{\gamma-2}e^{2\alpha\alpha^+}$$

$$+4Ae^{2\alpha\alpha^+}\sum_{r=0}^{\infty}\frac{(-2\alpha\alpha^+)^{r-1}}{(r-\gamma+1)r!} . \qquad (A18)$$

In the limit $\gamma=0$ it may be easily verified that (A18) reduces to (A15).

1. Normalization of the steady-state solutions

A normalization of the steady-state solutions is usually performed by setting the total probability to be 1 via the contour integral

$$\int_C d\alpha \int_{C'} d\alpha^+ P_s(\alpha,\alpha^+) = 1 . \qquad (A19)$$

Now since both (A15) and (A18) depend only on $N=\alpha\alpha^+$, we make the change of variables

$$N=\alpha\alpha^+, \quad z=\alpha ,$$

hence $\qquad\qquad\qquad\qquad\qquad\qquad\qquad (A20)$

$$d\alpha\,d\alpha^+ = z^{-1}dz\,dN .$$

Choosing a circular contour around the origin for the z integration we finally obtain

$$2\pi i \int_C P_s(N)dN = 1 . \qquad (A21)$$

(i) *Case $\gamma=0$.* The insertion of (A15) into (A21) gives

$$2\pi i \left[A\int_{C_1}\frac{1}{N^2}dN + B\int_{C_2}e^{2N}N^{-2}dN \right] = 1 . \qquad (A22)$$

The choice of a circular contour about the origin for C_1 makes the first integral zero, and for C_2 we choose a Hankel contour together with the relation[13]

$$\frac{2\pi i}{\Gamma(z)} = \int_{C_2}e^y y^{-z}dy \qquad (A23)$$

to give

$$2\pi i \left[A\times 0 + B\times\frac{4\pi i}{\Gamma(2)} \right] = 1 . \qquad (A24)$$

Therefore

$$B = \frac{\Gamma(2)}{2(2\pi i)^2} , \qquad (A25)$$

while A remains free.

(ii) *Case $\gamma\geq 0$.* Substituting (A18) into (A21) results in

$$2\pi i \left[4A\sum_{r=0}^{\infty}\frac{(-2)^{r-1}}{(r-\gamma+1)r!}\int_{C_i}e^{2N}N^{r-1}dN \right.$$

$$\left. + B\int_{C_2}e^{2N}N^{\gamma-2}dN \right] = 1 . \qquad (A26)$$

Now choosing both the contours to be Hankel paths, and noting that, because of the nature of the Γ function, all but the first term in the r sum are zero, we obtain the normalization requirement

$$B = \frac{\Gamma(2-\gamma)}{(\frac{1}{2})^{\gamma-1}(2\pi i)^2} + \frac{2A\,\Gamma(1-\gamma)}{(\frac{1}{2})^{\gamma-1}} . \qquad (A27)$$

Comparing the two cases we see that for $\gamma=0$, the nonzero probability current solution proportional to A contributes zero probability, but there is a finite addition from this as γ increases from zero.

2. Steady-state moments

These are calculated as

$$\langle(a^\dagger)^m a^n\rangle_s = \int_C d\alpha \int_{C'}d\alpha^+ \alpha^{+m}\alpha^n P_s(\alpha,\alpha^+) , \qquad (A28)$$

of which the most important in our case is the mean steady-state intensity

$$\langle a^\dagger a\rangle_s = \langle N\rangle_s = 2\pi i \int_C N^n P_s(N)dN , \qquad (A29)$$

where we have employed the change of variables (A20).

(i) *Case $\gamma=0$.* Following the same procedure as in Sec. 1 of this appendix we obtain

$$\langle N\rangle_s = 2\pi i \left[A\int_{C_1}\frac{1}{N}dN + B\int_{C_2}e^{2N}N^{-1}dN \right] \qquad (A30)$$

$$= \frac{(2\pi i)^2}{\Gamma(1)}B - 4\pi^2 A . \qquad (A31)$$

Substituting the value of B from (A25) gives the mean intensity result

$$\langle N\rangle_s = \tfrac{1}{2} - 4\pi^2 A . \qquad (A32)$$

(ii) *Case $\gamma\geq 0$:*

$$\langle N\rangle_s = 2\pi i \left[4A\sum_{r=0}^{\infty}\frac{(-2)^{r-1}}{(r-\gamma+1)r!}\int_{C_1}e^{2N}N^r dN \right.$$

$$\left. + B\int_{C_2}e^{2N}N^{\gamma-1}dN \right] . \qquad (A33)$$

With the choice of Hankel contours for C_1 and C_2, the first integral will always be zero, and the second integral gives

$$\langle N\rangle_s = \frac{(2\pi i)^2(\frac{1}{2})^\gamma}{\Gamma(1-\gamma)}B . \qquad (A34)$$

If we then substitute in for B from (A27), and cancel the Γ functions, we finally obtain

$$\langle N\rangle_s = \tfrac{1}{2}(1-\gamma) - 4\pi^2 A . \qquad (A35)$$

Comparing (A35) and (A32), the mean intensity changes continuously from one solution to the other as it must. The result (A35) predicts exactly the same steady-state dependence for $0\leq\gamma\leq 1$ as do the simulations in Sec. IV. However, there is another criterion to be placed on solutions, in addition to satisfying the generalized-potential conditions, before we can correctly predict steady-state moments. This is the requirement on the number-state probabilities and will be looked at in Sec. 3 of this appendix.

3. Number-state probabilities

The probability of the nth number state is given by $\langle n|\rho|n\rangle$, and is important to calculate since for an allowable steady-state distribution the probabilities must be all of the same sign. So using (A1) and the expansion of an arbitrary coherent state as

$$|\alpha\rangle = \sum_{s=0}^{\infty} \frac{e^{-\alpha\alpha^+/2}\alpha^s}{(s!)^{1/2}}|s\rangle \ , \tag{A36}$$

then it may be shown that the number-state probabilities are given by

$$\langle n|\rho|n\rangle = \int d\alpha \int d\alpha^+ \frac{e^{-\alpha\alpha^+}(\alpha\alpha^+)^n}{n!} P_s(\alpha,\alpha^+) \ . \tag{A37}$$

Again the integrand will always be a function of N so we make the change of variables (A20), and choose the z contour to be a circle around the origin, giving

$$\langle n|\rho|n\rangle = 2\pi i \int dN \frac{e^{-N}N^n}{n!} P_s(N) \ . \tag{A38}$$

(i) *Case* $\gamma = 0$:

$$\langle n|\rho|n\rangle = 2\pi i \left[\frac{A}{n!} \int_{C_1} e^{-N}N^{n-2}dN \right.$$
$$\left. + \frac{B}{n!} \int_{C_2} e^{N}N^{n-2}dN \right] , \tag{A39}$$

and choosing Hankel contours for both C_1 and C_2,

$$\langle n|\rho|n\rangle = \frac{(2\pi i)^2}{n!\Gamma(2-n)}[B - A(-1)^n] \ . \tag{A40}$$

(ii) *Case* $\gamma \geq 0$:

$$\langle n|\rho|n\rangle = 2\pi i \left[\frac{2A}{n!} \sum_{r=0}^{\infty} \frac{(-2)^{r-1}}{(r-\gamma+1)r!} \int_{C_1} e^{N}N^{n+r-1}dN \right.$$
$$\left. + \frac{B}{n!} \int_{C_2} e^{N}N^{n+\gamma-2}dN \right] \tag{A41}$$

$$= \frac{(2\pi i)^2}{n!} \left[\frac{B}{\Gamma(2-n-\gamma)} - \frac{A}{2(1-\gamma)\Gamma(1-n)} \right] , \tag{A42}$$

where we have used the standard Hankel contours and the properties of the Γ function for negative integers to obtain (A42).

We are now finally in a position to correctly determine the steady-state distributions of the system. For $\gamma = 0$, (A40) shows that we obtain a nonoscillating set of solutions providing $|A| < |B|$. It also confirms that the only $|0\rangle$ and $|1\rangle$ number states have nonzero probabilities in the steady states. The mean intensity will be given by (A32) where A is now bounded by the probability requirement above. We still have the novel feature that the solution proportional to A contributes zero probability [refer to (A22)] but does have an effect on the mean. The value of A is not exactly specified by the probability requirements, but instead would depend on the imposed initial condition for the intensity. For large initial conditions we would expect the most probable value of A to be zero, in which case $\langle N\rangle_s = \frac{1}{2}$, the ground and first number states having equal probability in the stationary state.

For $\gamma > 0$ the effect is more striking. Due to the oscillatory nature of the Γ function in (A42), B must be zero in order to prevent the appearance of nonzero probability number states with opposite signs. In this case we then only obtain a nonzero probability for the ground state as we physically require. As shown in Sec. II of this appendix the A solution now has finite probability and can be normalized. However, putting $B=0$ into (A34) gives $\langle N\rangle_s = 0$ so that the complex P representation provides results in accordance with our physical expectations and the jump process simulation.

Finally, we should note that this analysis explicitly excludes nonzero integral values for γ, but it may be shown that the mean intensity for these cases is also zero in the steady state using the complex P representation.

[1]H. J. Carmichael, J. S. Satchell, and S. Sarkar, Phys. Rev. A **34**, 3166 (1985); M. Wolinsky and H. J. Carmichael (unpublished); K. J. McNeil and I. J. D. Craig (unpublished).

[2]P. D. Drummond and C. W. Gardiner, J. Phys. A **13**, 2353 (1980).

[3]J. R. Klauder and W. P. Petersen, SIAM (Soc. Ind. Appl. Math.) J. Numer. Anal. **22**, 1153 (1985).

[4]K. M. McNeil and I. J. D. Craig (unpublished).

[5]M. Wolinsky and H. J. Carmichael (unpublished).

[6]W. H. Louisell, *Quantum Statistical Properties of Radiation* (Wiley, New York, 1973); derivation of master equation in Markov approximation, pp. 335–368.

[7]C. W. Gardiner, *Handbook of Stochastic Methods* (Springer-Verlag, Berlin, 1983); transformations are found for the many-variable case on p. 100. These are generalized by replacing $\frac{1}{2}$ with θ_2.

[8]W. Rumelin, SIAM (Soc. Ind. Appl. Math.) J. Numer. Anal. **19**, 604 (1982).

[9]Spikes have been experienced in all the works of Ref. 1.

[10]H. J. Carmichael, J. S. Satchell, and S. Sarker, Phys. Rev. A **34**, 3166 (1985).

[11]C. W. Gardiner, Ref. 7; the general solution of a single variable linear equation is found on pp. 112 and 113.

[12]C. W. Gardiner, Ref. 7; given as theorem on p. 412, Eq. (10.6.15).

[13]A. Erdelyi, *Higher Transcendental Functions* (McGraw-Hill, New York, 1953), Vol. 1; this formula is found on p. 13.